Article

pubs.acs.org/Biomac

Electrochemiluminescence Biosensor Based on Conducting Poly(5-formylindole) for Sensitive Detection of Ramos Cells

Guangming Nie,* Zhimin Bai, Wenying Yu, and Juan Chen

State Key Laboratory Base of Eco-chemical Engineering, College of Chemistry and Molecular Engineering, Qingdao University of Science and Technology, Qingdao 266042, People's Republic of China

Supporting Information

ABSTRACT: A signal-on electrochemiluminescence (ECL) biosensor devoted to the detection of Ramos cells was fabricated based on a novel conducting polymer, poly(5-formylindole) (P5FIn), which was synthesized electrochemically by direct anodic oxidation of 5-formylindole (5FIn). This ECL platform was presented by covalently coupling the 18-mer amino-substituted oligonucleotide (ODN) probes with aldehyde groups that are strongly reactive toward a variety of nucleophiles on the surface of solid substrates. The specific identification and high-affinity between aptamers and target cells, gold nanoparticles (AuNPs) enhanced ECL nanoprobes, along with P5FIn induced ECL quenching contributed greatly to the sensitivity and selectivity. The ECL signals were logarithmically linear with the concentration of Ramos cells in a wide determination range from 500 to 1.0×10^5 cells mL^{-1}, and the corresponding detection limit was 300 cells mL^{-1}.

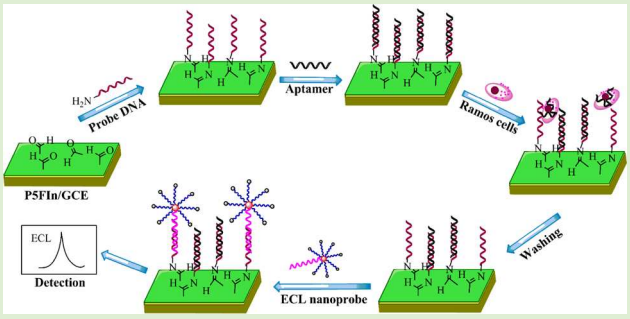

INTRODUCTION

In the past three decades, the sustained growth tendency of deaths from cancer has made it a leading threat to human beings. Therefore, within the perspective of manifestly improving the recovery rates of cancer, the research on accurate and sensitive identification and detection of cancer cells is of great importance to the early diagnosis and prompt exactitude therapy. Typically, some current available approaches including polymerase chain reaction (PCR), flow cytometry, and cytopathological examination have been employed for high-rate detection of cancer cells.[1] Nevertheless, there are some disadvantages for these methods, such as the requirement of sophisticated instrumentation and qualified personnel combined with additional procedures to enrich target cells or express fluorescent protein in the cells, which in turn give rise to the consumption of cost, labor, and time. Thus, extensive efforts have been made to meet the increasing demands for biosensors with good sensitivity and selectivity, as well as miniaturization and low cost.[2] So far, successful detection and identification of cancer cells have been achieved by assays associated with diversified techniques such as quartz crystal microbalance (QCM),[3] electrochemical,[4−6] fluorescence,[7,8] microfluidics,[9,10] or chemiluminescence (CL)[11] methods.

Electrochemiluminescence (ECL), one kind of CL, has been widely concerned in the field of biosensing application in recent years, owing to its intrinsic advantages of high sensitivity, excellent selectivity, good reproducibility, wide range of analytes, and low cost.[12−16] Among the various existing ECL systems, the most widely applied ECL system is the $Ru(bpy)_3^{2+}$ (or its derivatives)/TPA system based on an "oxidative−reductive" coreactant pathway because of its superior properties such as high efficiency, fast response and good stability of ECL emissions exhibited in aqueous solutions.[12,13] Particularly, for most biomolecules detected in a $Ru(bpy)_3^{2+}$/TPA system, such as protein, DNA, and peptide, their ECL assays are mainly accomplished by solid phase ECL detection formats, where biomolecules should be immobilized on a solid substrate, typically an electrode. A variety of methods based on electrostatic adsorption,[17] physical entrapment,[18] affinity interactions,[19,20] and covalent coupling immobilization[21−23] have been developed for biomolecules fastening on solid substrates up to now. Among these, the covalent coupling approach can exhibit several fascinating features[12] like good stability, high reproducibility, and less nonspecific adsorption surfaces for ECL detection.

Nowadays, conducting polymers (CPs) have attracted more and more attention due to some unique properties, including rapid electron transfer, specificity, high sensitivity, and biocompatibility.[24−26] These functional materials can not only act as suitable immobilization carriers for biomolecules, but also have active effects on the transduction of biosensors and, thus, can be used as valid interfaces between the nucleic acids and the electronic transducers. Especially CPs with reactive functionalities can facilitate the covalent immobilization, and the formed conductive substrates can sensitively indicate a biological

Received: December 7, 2012
Revised: January 30, 2013
Published: February 4, 2013

Table 1. Base Sequences of Oligonucleotides Involved in This Work

name	sequence
probe DNA S1	5′-NH_2-$(CH_2)_6$-AGGCGTGGCTATTCCCAA-3′
Ramos cells aptamer	5′-TAGGCAGTGGTTTGACGTCCGCATGTTGGGAATAGCCACGCCT-3′
binding DNA S2	5′-SH-$(CH_2)_6$-TTTTTTCCCGCGCGCTTGGGAATAGCCACGCCT-3′
linker DNA S3	5′-SH-$(CH_2)_6$-TTTTTTTTTTT-$(CH_2)_6$-NH_2-3′

recognition event, such as DNA hybridization. As a consequence, functionalized CPs, typically the ones bearing functionalized carboxylic acid have been widely employed in the fabrication of biosensors[27−29] because the carboxylic functional groups can act as a precursor for the covalent binding of biomolecules modified with amino terminals. The carboxylic groups are, however, somewhat inert at ambient temperature and, hence, activation by chemical agents (EDC and NHS) is normally exploited to increase the efficiency of the peptide-formed conjugation. Based on these considerations, we expect to shift focus to CPs containing aldehyde groups, because the aldehyde groups (an acceptor) are strongly reactive toward a variety of nucleophiles.[30−32] More than that, the introduction of aldehyde groups can improve the solubility, thermal stability, and optoelectronic properties of the materials, which extends their applications in the biosensing or drug delivery realms. Haddleton and co-workers[33] have reported the synthesis of α-aldehyde-terminated poly(methoxyPEG) methacrylates from Cu(I) mediated living radical polymerization and their efficient conjugation to lysozyme as a model protein. As the polypyrrole[34,35] and polythiophene derivatives[36−38] have been the most commonly investigated CPs for biosensor applications, our group is currently concerned with the polyindole family considering its several advantages, especially fairly good thermal stability, high redox activity, and stability.[39−41]

In this article, we first reported a signal-on ECL biosensor based on a novel poly(5-formylindole) (P5FIn) film using a ruthenium complex, ruthenium bis(2,2′-bipyridine) (2,2′-bipyridine-4,4′-dicarboxylic acid) *N*-hydroxysuccinimide ester [$Ru(bpy)_2$(dcbpy)NHS], as a label. The precursor polymer with good electroactivity, high conductivity, and excellent optoelectrochemical properties can be readily prepared by direct electrochemical polymerization of the 5-formylindole (5FIn) monomers on a solid glassy carbon electrode (GCE) in one step. The 18-mer amino-substituted oligonucleotide (ODN) probes were covalently immobilized to the surface of the solid substrates by an aldimine condensation pathway. The hybridization of aptamers and probe DNA S1, then the specific recognition between aptamers and their target cells, followed by the binding of labeled probes realized the detection of ECL signals. In design of herein proposed sensor, the gold nanoparticles (AuNPs) enhanced ECL nanoprobes tagged with $Ru(bpy)_2$(dcbpy)NHS served as not only a target recognition element but also a tool of amplification. Interactions between aptamers and their targets (such as small peptides, organics, proteins, cells, and even bacteria) tend to be extremely specific, and the unique binding affinities can range from the picomolar scale (10^{-12} M) to a high-micromolar scale (10^{-6} M).[42] In addition, it has been demonstrated that CPs have quenching effects on the luminescence signals of any species if they appear in close proximity (less than nm) to their surface,[43,44] so nonspecifically adsorbed ECL exhibiting compounds within analyte detection can be quenched by P5FIn matrix surface. All of these vantage points make sense for the highly sensitive and selective detection of Burkitt's lymphoma (Ramos).

EXPERIMENTAL SECTION

Reagents and Materials. Oligonucleotides (ODNs) were synthesized by SBS-bio Genetech. Co. Ltd. (China). Their base sequences were listed in Table 1. 5-Formylindole (5FIn, 98%) was obtained from Frontier Scientific; Ruthenium(III) chloride hydrate ($RuCl_3 \cdot xH_2O$, 99.9%), 2,2′-bipyridine (99%), 2,2′-bipyridyl-4,4′-dicarboxylic acid (dcbpy, 98%), and chloroauric acid ($HAuCl_4$) from Acros Organics (Japan); *N*,*N*′-dicyclohexyl carbodiimide (DCC, 99%), *N*-hydroxysuccinimide (NHS, 99%), and sodium hexafluorophosphate ($NaPF_6$, 98.5+%) from Sigma (U.S.A.); tripropylamine (TPA) from Adrich (U.S.A.); acetonitrile (ACN, 99.5%) from Tianjin Bodi Chemical Corporation (Tianjin, China); and trisodium citrate from Shanghai Reagent Company (Shanghai, China) were used as received. Tetrabutylammonium tetrafluoroborate (TBATFB, Acros Organics, 98%) was dried in vacuum at 60 °C for 24 h before use. All other reagents were of analytical grade and used as received. Doubly distilled water (DDW) was used throughout the work.

Ramos cells (CRL-1596, B-cell, human Burkitt's lymphoma) and Hela cells were obtained from the Chinese Academy of Medical Sciences. The cells were cultured in RPMI 1640 medium supplemented with 10% fetal bovine serum (FBS) and 100 IU mL^{-1} penicillin streptomycin. The cell density was determined by using a hemocytometer, and this was performed prior to any experiments. Approximately one million cells dispersed in RPMI 1640 cell media buffer were centrifuged at 3000 rpm for 5 min and redispersed in cell media three times and were then redispersed in cell media buffer (1 mL). During all experiments, the cells were kept in an ice bath at 4 °C.

Apparatus. Electrochemical deposition and cyclic voltammetry measurement were carried out in a Model 263 potentiostat−galvanostat (EG&G Princeton Applied Research). Electrochemical impedance spectrum (EIS) was recorded with a model 660C Electrochemical Analyzer (CH Instruments). The ECL responses were detected by a model MPI-A electrochemiluminescence analyzer (Xi'An Remax Electronic Science and Technology Co. Ltd., Xi'An, China) with a voltage of +800 V supplied to the photomultiplier tube (PMT). The working and counterelectrodes were GCE (3.0 mm in diameter, 7.0 mm^2 in geometrical area) and platinum-wire electrode, respectively. The reference electrode was Ag/AgCl/KCl (satd) to which all potentials were referred. UV−visible spectra were taken by using Cary 50 UV−vis−NIR spectrophotometer. Scanning electron microscopy (SEM) measurements were taken using a JEOL JSM-6700F instrument.

Electrosynthesis of P5FIn Films. Electrochemical synthesis and examinations were carried out in a one-compartment cell with the use of a Model 263 potentiostat−galvanostat (EG&G Princeton Applied Research) under computer control. Prior to the electropolymerization, the working electrode GCE was polished with 1.0, 0.3, and 0.05 μm alumina slurry successively, then rinsed with DDW after each polishing step, and finally cleaned ultrasonically in 95% ethanol and water in turn.

The typical electrolyte was ACN containing 0.05 M 5FIn monomers and 0.1 M TBATFB. All solutions were deaerated by a dry argon stream and maintained at a slight argon overpressure during experiments. The thickness of the polymer film deposited on the electrode was controlled by monitoring the amount of charge passed during the polymerization process. To remove the electrolyte and oligomers/monomers, the achieved P5FIn films were rinsed with acetone first and then with pH 7.4 PBS.

Scheme 1. Electropolymerization of P5FIn Films (a) and the ECL Biosensor Based on P5FIn Films Using AuNP Enhanced Nanoprobes for Signal-on Detection of Ramos Cells (b)

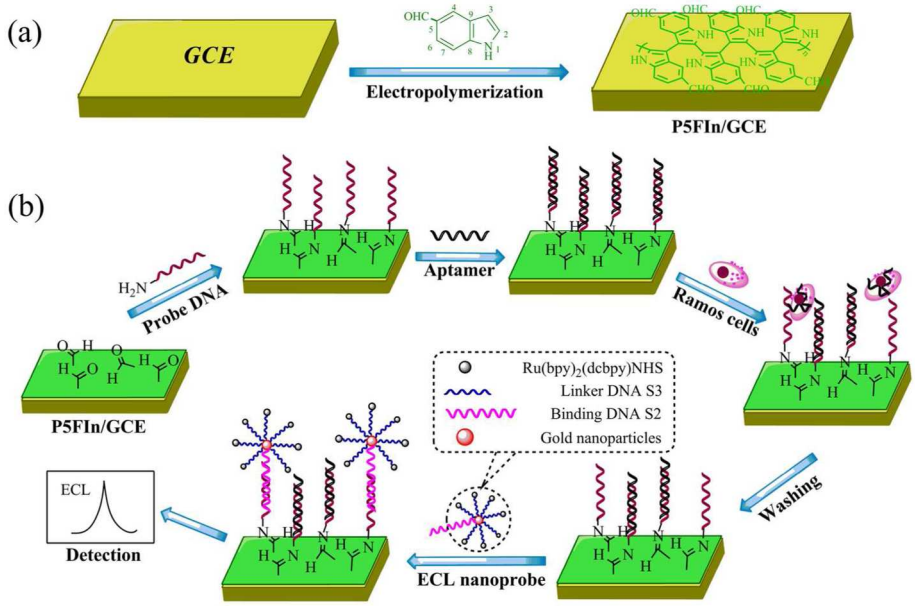

Labeling of ECL Signal Probes. $Ru(bpy)_2(dcbpy)NHS$ was prepared referring to previously published protocols,[45,46] with slight modifications, as needed. The ECL signal probes (denoted as Ru−S3) were prepared in accordance with reference[45] (see more details in Supporting Information).

Preparation of the AuNP Enhanced ECL Nanoprobes. AuNP with average diameter of 15 nm were synthesized through the reduction of $HAuCl_4$ by trisodium citrate according to the previously published methods.[47,48] The ECL nanoprobes (denoted as Ru−DNA−Au NPs) were synthesized consulting the protocol published,[49,50] with slight modifications (details are shown in Supporting Information).

Fabrication of the ECL Biosensor. The P5FIn modified GCE was primarily immersed into pH 6.0 PBS containing 0.10 μM S1 for about 1 h to produce a S1/P5FIn attached GCE. Then, the electrode was incubated in 0.1 M PBS (pH 7.4) containing 1.0 μM aptamers for 3 h at 37 °C, followed by dipping the formed aptamer/S1/P5FIn/GCE into solution of Ramos cells with different concentrations. The specific identification between aptamers and Ramos cells was conducted at 37 °C for 1.5 h so as to liberate S1. In order to remove free oligonucleotides or nonspecifically adsorbed species, the electrode was thoroughly washed with pH 7.4 PBS and DDW for several times after each step. Finally, the Ru−DNA−Au NPs were assembled onto the surface of modified GCE via the hybridization events between S2 and S1 (Scheme 1).

ECL Detection. After washing to remove unbound ECL nanoprobes with the same buffer, the resulting electrode was immersed in 0.1 M PBS (pH 7.4) containing 0.1 M TPA for a typical ECL test. With a scan rate of 100 mV s^{-1}, the linear scan potential was applied between 0 and +1.30 V, and the voltage of the PMT was operated at +600 ~ +800 V. ECL signals related to the Ramos cells concentrations could be measured.

RESULTS AND DISCUSSION

Electrochemical Polymerization of 5FIn. Successive cyclic voltammetry (CV) in the form of current−potential diagrams is a valid and visualized method for investigating the reversibility and electroactivity of the polymer. The cyclic voltammograms (CVs) of 5FIn monomers in ACN with 0.1 M TBATFB as supporting electrolyte were shown in Figure 1. As can be seen from Figure 1, on the first CV curve, the current densities on the reverse scan were higher than that on the forward scan (1.2−1.6 V vs Ag/AgCl), which could be explained as the characteristic of nucleation process.[51−54] With the CV scan continued, the gradual increase in the redox couple currents implied that the amount of the polymer (measured by the polymerization charge[55]) on the electrode was increasing. All these phenomena indicated that a high-quality conducting P5FIn film was formed on the working electrode.

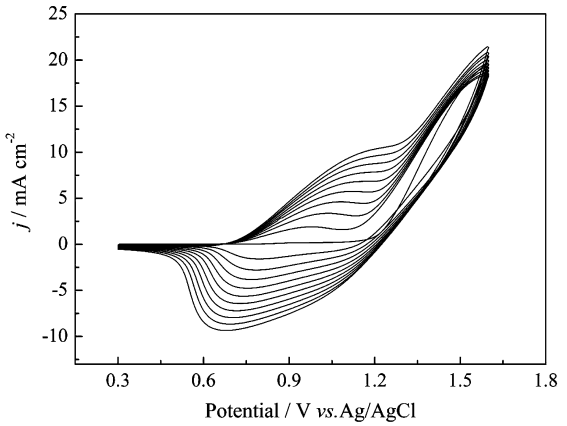

Figure 1. Cyclic voltammograms of 0.05 M 5FIn monomers. Potential scan rate: 100 mV s^{-1}. Polymerization charge density: 0.8 C cm^{-2}.

Characterization of P5FIn Films. Viewed by structure, the indole monomer contains a benzene ring and a pyrrole ring, whereupon the polyindole can be regarded as a copolymer of benzene and pyrrole monomers in some extent. As discussed in our previous work,[56] the conductivity of P5FIn films was measured to be 2.43×10^{-2} S cm^{-1} at room temperature, and the polymer also displayed a high electrochemical activity and stability in both monomer-free ACN solution and concentrated sulfuric acid. Thermal analysis revealed that the thermal decomposition of P5FIn happened from 700 to 800 K, with a weight loss of merely 15%. When the temperature was up to

dx.doi.org/10.1021/bm3018802 | Biomacromolecules 2013, 14, 834−840

1100 K, the residue of P5FIn was about 70%, indicating high thermal stability. Fluorescent spectral studies indicated that P5FIn was a good green-light-emitter with high fluorescence quantum yield and photochemical stability. Such high thermal stability and excellent electro-optical properties of P5FIn films were mainly caused by the substitution of aldehyde group in the benzene ring. From a scientific point of view, all these advantageous properties indicated that P5FIn might be a promising candidate for biosensing application.

Electrochemical and Morphological Characterization of S1/P5FIn/GCE. Owing to the strong reactivity toward a variety of nucleophiles, abundant aldehyde groups can improve the hydrophilicity of polymer films[34] deposited on the electrode surface while enabling biomolecules immobilization via covalent bonding. In our strategy, the probe DNA S1 functionalized with an amino group at the 5′-end was covalently immobilized on the P5FIn matrix. The conjugation reaction was carried out in faintly acid circumstances[33] so as to facilitate the formation of the imino linkage between the polymer and the ODNs without utilizing EDC/NHS catalysts.

With the purpose of verifying the attachment of S1 onto P5FIn main chains, CV was first used to investigate the electron transfer behavior tunneling through the barrier layers of the modified electrode. CVs of the stepwise fabrication process of the sensing interface were first recorded in 0.1 M NaCl aqueous solution containing 1.0×10^{-4} M $K_3Fe(CN)_6$ as the electroactive marker (Figure 2). As shown in Figure 2, the

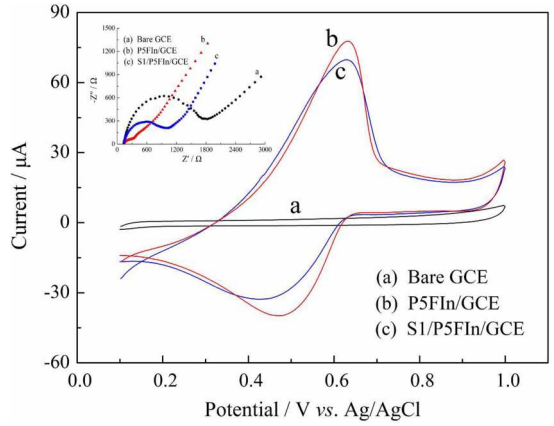

Figure 2. CVs of the bare GCE (a) and P5FIn-coated GCE before (b) and after (c) modified with probe DNA S1. Scan rate: 100 mV s^{-1}. Inset: EIS spectra of the stepwise fabrication process.

CV curve of $Fe(CN)_6^{3-}$ recorded on the P5FIn/GCE (curve b) indeed displayed a considerable increase of peak currents compared with that of bare GCE (curve a). This could be attributed to the porous structure and relatively high conductivity of the films, which efficiently boosted the electrons of $Fe(CN)_6^{3-}$ transfer through the P5FIn matrix.[57] After the immobilization of S1, the peak currents decreased and the redox peak potentials presented a slight negative shift. In addition, the peak-to-peak potential separation increased (ΔE = 200 mV) in comparison with that of the P5FIn/GCE (ΔE = 160 mV), which might be due to the electrochemical reaction on the electrode interface blocked by the electrostatic repulsion between the negatively charged ODNs and the anionic ferricyanide.[58,59] Besides the CV, the conjugated attachment was also studied with EIS in the aqueous solution of 2 mM $Fe(CN)_6^{4-}/Fe(CN)_6^{3-}$ (inset, Figure 2). The spectra were illustrated in the form of Nyquist plots, in which the semicircles at high frequencies corresponded to the electron-transfer-limited process with its diameter equaling to the electron transfer resistance (Ret), while the straight lines at low frequencies were aroused by the diffusion control of the reactant species.[34] It was clear that the diameter of semicircle of P5FIn/GCE (curve b) was dramatically smaller than that of the bare GCE (curve a), indicating a noticeable decrease (~80%) in the electron transfer resistance, which should give the credit to high electrode coverage of P5FIn layer. Then, the resistance increased to 870 Ω after the immobilization of probe DNA S1 (curve c), due to the obstructive behavior of ODNs for interfacial electron transfer process.[57] All these results were in coincidence with the CVs, indicating that the probe DNA S1 had been successfully immobilized onto P5FIn modified electrode.

To further validate the coupling process with morphological analysis, SEM was utilized for characterizing the multilayer construction process of the sensing substrate. It can be seen from the SEM images that P5FIn film (Figure 3A) was loosely

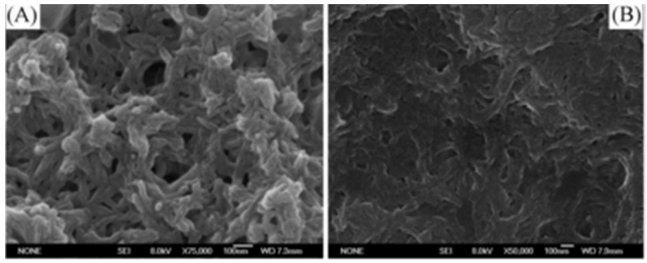

Figure 3. Scanning electron micrographs of P5FIn/GCE (A) and S1/P5FIn/GCE (B).

packed porous structure in the form of net-like morphology, which could facilitate the ion transport during the redox reactions and provide larger surface areas for the covalent binding of amino-substituted ODN probes. In the case of S1/P5FIn film modified electrode, however, the surface exhibited a change of three-dimension architecture with less porous structure and more uniform morphology (Figure 3B). This uniform three-dimension interface could hinder the rate of electron transfer between the electrode interface, whereas increase the electron transfer resistance, which were consistent with CV and EIS characterizations. It should be noted that the incorporation of probe DNA with P5FIn matrix could offer a molecular scale analogue texture for further DNA hybridization.[60] We thereupon gained the green light to proceed with the following procedures.

Characterization of the ECL Nanoprobes. The ECL nanoprobes, synthesized according to the process described in the Experimental Section, were characterized by UV−vis spectrophotometry (UV−vis absorption spectra were shown in Figure S1, Supporting Information). The results indicated that both S2 and Ru−S3 had been bound to AuNP.

The ECL behavior of ECL nanoprobes was also investigated at the prepared P5FIn/GCE in the presence of TPA. It was found that the ECL intensity reached the maximum when a constant potential of +1.30 V was employed. Hence, an applied constant potential of +1.30 V was chosen in this system in view of its excellent sensitivity. As shown in Figure 4, the preprocessing P5FIn/GCE labeled with $Ru(bpy)_2(dcbpy)NHS$ showed an incisive ECL response at the applied potential, along

dx.doi.org/10.1021/bm3018802 | Biomacromolecules 2013, 14, 834−840

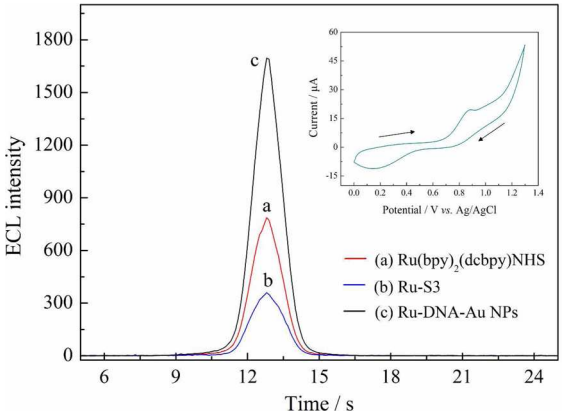

Figure 4. ECL intensity vs time profiles obtained in 0.1 M PBS (pH 7.4) containing 0.1 M TPA: 4.8×10^{-8} M $Ru(bpy)_2(dcbpy)NHS$ (a), 2.4×10^{-8} M Ru–S3 (b), and 4.4×10^{-11} M Ru–DNA–AuNPs (c). Inset: CV curve of the $Ru(bpy)_2(dcbpy)NHS$ modified GCE in the same solution. Scan rate: 100 mV s^{-1}.

with a good redox property[61] from +0.85 V to +1.15 V (inset, Figure 4). The general oxidation reduction mechanism of $Ru(bpy)_3^{2+}$/TPA ECL system were illustrated in Scheme 2.[62]

Scheme 2. General Oxidation Reduction Mechanism of $Ru(bpy)_3^{2+}$ with TPA as the Co-Reactant

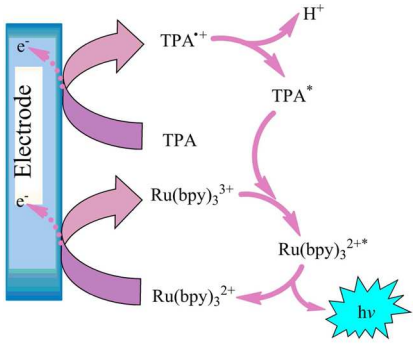

To our amazement, however, the ECL intensity of Ru–S3 was nearly 5-fold lower than that of $Ru(bpy)_2(dcbpy)NHS$ at the same concentration, which declared a decrease of ECL efficiency. This result could be explained by the decrease in the diffusion coefficient of Ru–S3 originated from the increase of the molecular weight.[46] Nevertheless, the ECL emission had a dramatic rise after connecting the ECL signal probes and binding DNA S2 to AuNP, which could be attributed to the remarkable amplification of AuNP. Consequently, the conclusion came down to us that the AuNP enhanced nanoprobes had been successfully synthesized and displayed a fine ECL performance.

Signal on ECL Measurement of Ramos Cells. Figure 5A illustrated the ECL profiles of different concentrations of Ramos cells measured by the ECL biosensor under the optimized condition of 0.10 M PBS (pH 7.4) containing 0.10 M TPA. As shown in Figure 5A, the ECL signals were in response to changes of target cell concentration, more specifically, the ECL emission intensity gradually enhanced with the increase of Ramos cell concentration. With respect to the principle of detection and quantitation (Scheme 1), briefly, when immersing the fabricated biosensor into the solution of Ramos cells, the cells would be captured onto electrode via the

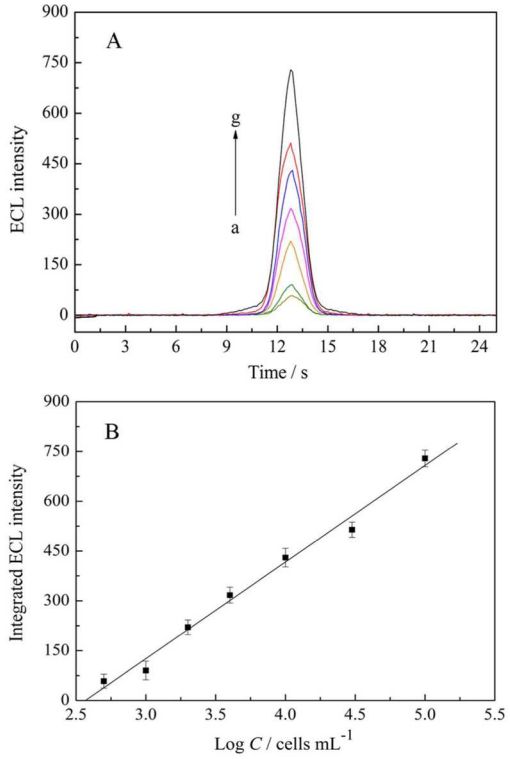

Figure 5. (A) ECL profiles of the different concentration of Ramos cells: (a) 500, (b) 1×10^3, (c) 2×10^3, (d) 4×10^3, (e) 1×10^4, (f) 3×10^4, and (g) 1×10^5 cells mL^{-1}. (B) Linear relationship (n = 7) between ECL emission and logarithm of Ramos cell concentration. Error bars were obtained from three parallel experiments.

specific recognition and high affinity between aptamers and cell surface carbohydrates. As the avidity-mediated interaction (or dissociation constant) of aptamer-cell complexes was stronger than the hydrogen bonds formed by complementary bases, the double-stranded (ds) DNA underwent a conformational change and dehybridized in the presence of the target analyte so that the probe DNA S1 was released as a result. Subsequently, the Ru–DNA–Au NPs were tagged to the electrode surface by means of hybridization events between the complementary sequences of binding DNA S2 and probe DNA S1 and, finally monitored by an ECL detector. Thus, the ECL responses were indirectly bound up with the number of cells recognized by apatmers and we could determine the cell concentration with ECL measurement.

According to Figure 5B, the integrated ECL intensity was positively related to the logarithmic value of cell concentration in the range from 500 to 1.0×10^5 cells mL^{-1}. The linear regression equation was $I = -747.03 + 290.97 \log C$ (unit of C is cells mL^{-1}) with a correlation coefficient of 0.9937. The detection limit of this P5FIn-based ECL biosensor for Ramos cells was calculated to be 300 cells mL^{-1} at 3σ, which was lower than some reported sensors.[6,63,64] Furthermore, the analytical performance of the proposed sensor has been compared with several other recently reported cytosensors in characteristics such as linear range and detection limit (Table 2). Though the sensitivity of our protocol for Ramos cell detection is not superior to the published works based on fluorescent nanoclusters[65] and magnetic nanoparticles,[66] the advantages of miniaturization, simplicity, and low-cost still provide new insights into the fabrication of P5FIn-based biosensors by an ECL reader. Further improvements of the sensitivity may be

dx.doi.org/10.1021/bm3018802 | Biomacromolecules 2013, 14, 834–840

Table 2. Comparison of Our Biosensor with Several Other Bioensors for Cell Detection (Units: Cells mL^{-1})

cell detection methods or techniques	cell lines	liner range	detection limit
P5FIn-based electrochemiluminescence biosensor	Ramos	$500-1.0 \times 10^5$	300
graphene-functionalized electrochemical aptasensor[6]	Hela	$0-1.0 \times 10^6$	1000
electrochemical immunoassay[63]	MCF-7	$1.6 \times 10^3-2.0 \times 10^5$	700
3-D architectured electrochemical immunosensor[64]	Hela	$8.0 \times 10^2-2.0 \times 10^7$	500
CdSe nanoclusters amplified fluorescence biosensor[65]	Ramos	$50-1.0 \times 10^3$	50
aptamer-conjugated magnetic nanosensor[66]	CCRF-CEM	$4-4.0 \times 10^6$	40

achieved by employing more sensitive composites of P5FIn with nanomaterials (such as nanoparticles and multiwall carbon nanotubes). To evaluate the feasibility of the ECL biosensor for actual applications, whole blood was used as a model biological media to mimic a real disease state. The detection of Ramos cells in whole blood was performed by incubating Ramos cell-spiked media with the fabricated biosensor. The resulting calibration plot (Figure S3, Supporting Information) of the ECL signals was in proportion to the logarithm of the number of the Ramos cells over a range of 1000 to 2.0×10^4 cells mL^{-1} and was suitable for quantitative work.

As shown in Figure 6, no obvious change was observed from the ECL emission-time curves when the ECL biosensor was

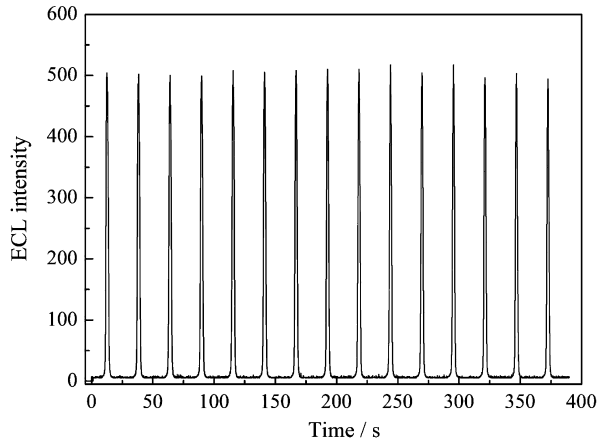

Figure 6. ECL responses of P5FIn/S1/aptamers/Ru–DNA–Au NPs upon continuous 15-cyclic scans between 0 and +1.30 V in 0.1 M PBS (pH 7.4) containing 0.1 M TPA. Scan rate: 100 mV s^{-1}.

successively scanned for 15 cycles in the potential range between 0 and +1.30 V at a scan rate of 100 mV s^{-1}, indicating that the fabricated multisignal responsive biosensing interface possessed an excellent potential cycling stability. Meanwhile, the precision for detection of target cells with the designed ECL biosensor was also evaluated by using a series of four replicated measurements of 4000 cells mL^{-1}, and the relative standard deviation (RSD) was 4.68%, showing good reproducibility.

To appraise the selectivity of the ECL biosensor, the control experiment was performed with HeLa cells at the same concentration (4000 cells mL^{-1}) with Ramos cells. The ECL response was almost the same with the blank without cells (Figure S4, Supporting Information), indicating a good selectivity for Ramos cell detection in the buffer system. Further detection of Ramos cell-spiked whole blood (4000 cells mL^{-1}) was carried out to demonstrate the specificity of this biosensor in a real clinic state. As shown in Figure S4, the ECL signal of Ramos cells obtained from biological media (column d) was slightly lower than that in buffer system (column a), probably due to the nonspecific interactions caused unwanted aggregates of interference species on the cells' surfaces. Overall, the developed biosensor showed a good selectivity for Ramos cells in both buffer system and biological media.

CONCLUSIONS

We have designed a sensitive ECL biosensor based on a novel substrate prepared by covalently coupling of an amino-substituted oligonucleotide to a high-quality conducting P5FIn film obtained from direct electrochemical oxidation of the 5FIn monomers. This newly constructed platform offered high sensitivity and good selectivity for Ramos cells and possessed a low detection limit of 300 cells mL^{-1}. Such excellent performances mainly benefit from several significant advantages of the material and method: (1) abundant aldehyde groups (an acceptor) improve the hydrophilicity of the polymer film on the electrode surface and the porous structure provided by P5FIn films offers larger specific surface area, which greatly increases the amount of biomolecules assembled onto the surface of the electrode; (2) the high positive potential of +1.30 V versus Ag/AgCl applied at the electrode during the ECL measurement has synergistic effects on the conductivity of the sensitive element, herein, the conducting P5FIn films; (3) the high specificity and affinity of aptamers to target cells and the AuNPs enhanced nanoprobes employed in the assays are much favored for the improvement of selectivity and sensitivity. This ECL biosensor affords a promising method for the detection and quantification of Ramos cells, thus, broadens the application fields of conducting polymers in clinical diagnosis and actual application of the assay.

ASSOCIATED CONTENT

Supporting Information

Synthesis experiments, UV–vis spectra, detection conditions, and detection results. This material is available free of charge via the Internet at http://pubs.acs.org.

AUTHOR INFORMATION

Corresponding Author

*E-mail: gmnie@126.com. Tel.: +86-532-88956556. Fax: +86-532-88957187.

Notes

The authors declare no competing financial interest.

ACKNOWLEDGMENTS

The authors thank the Scientific Research Startup Foundation of QUST for talents, the Scientific and Technical Development Project of Qingdao (11–2–4–3–(10)–jch), China Postdoctoral Science Foundation (2012M521288), and Natural Science Foundation of Shandong Province (No. ZR2011BM003).

REFERENCES

(1) Paterlini-Brechot, P.; Benali, N. L. *Cancer Lett.* **2007**, *253*, 180–204.

(2) Liu, G. D.; Mao, X.; Phillips, J. A.; Xu, H.; Tan, W. H.; Zeng, L. W. *Anal. Chem.* **2009**, *81*, 10013−10018.
(3) Apodaca, D. C.; Pernites, R. B.; Ponnapati, R. R.; Del Mundo, F. R.; Advincula, R. C. *ACS Appl. Mater. Interfaces* **2011**, *3*, 191−203.
(4) Chikkaveeraiah, B. V.; Bhirde, A. A.; Morgan, N. Y.; Eden, H. S.; Chen, X. *ACS Nano* **2012**, *6*, 6546−6561.
(5) Wang, R.; Di, J.; Ma, J.; Ma, Z. *Electrochim. Acta* **2012**, *61*, 79−184.
(6) Feng, L. Y.; Chen, Y.; Ren, J. S.; Qu, X. G. *Biomaterials* **2011**, *32*, 2930−2937.
(7) Rejinold, N. S.; Chennazhi, K. P.; Tamura, H.; Nair, S. V.; Jayakumar, R. *ACS Appl. Mater. Interfaces* **2011**, *3*, 3654−3665.
(8) Yuan, L.; Lin, W.; Zhao, S.; Gao, W.; Chen, B.; He, L.; Zhu, S. *J. Am. Chem. Soc.* **2012**, *134*, 13510−13523.
(9) Sheng, W.; Chen, T.; Kamath, R.; Xiong, X.; Tan, W.; Fan, Z. H. *Anal. Chem.* **2012**, *84*, 4199−4206.
(10) Hanke, C.; Dittrich, P. S.; Reyes, D. R. *ACS Appl. Mater. Interfaces* **2012**, *4*, 1878−1882.
(11) Zong, C.; Wu, J.; Wang, C.; Ju, H. X.; Yan, F. *Anal. Chem.* **2012**, *84*, 2410−2415.
(12) Miao, W. J. *Chem. Rev.* **2008**, *108*, 2506−2553.
(13) Qi, H. L.; Peng, Y. G.; Gao, Q.; Zhang, C. X. *Sensors* **2009**, *9*, 674−695.
(14) Zhao, Z.; Zhou, X.; Xing, D. *Biosens. Bioelectron.* **2012**, *31*, 299−304.
(15) Forster, R. J.; Bertoncello, P.; Keyes, T. E. *Annu. Rev. Anal. Chem.* **2009**, *2*, 359−385.
(16) Wu, M. S.; Qian, G. S.; Xu, J. J.; Chen, H. Y. *Anal. Chem.* **2012**, *84*, 5407−5414.
(17) Uto, K.; Yamamoto, K.; Kishimoto, N.; Muraoka, M.; Aoyagi, T.; Yamashita, I. *J. Mater. Chem.* **2008**, *18*, 3876−3884.
(18) David, A. E.; Yang, A .J; Wang, N. S. *Methods Mol. Biol.* **2011**, *679*, 49−66.
(19) Jeon, S. D.; Lee, J. E.; Kim, S. J.; Kim, S. W.; Han, S. O. *Biosens. Bioelectron.* **2012**, *35*, 382−389.
(20) Mori, Y.; Minamihata, K.; Abe, H.; Goto, M.; Kamiya, N. *Org. Biomol. Chem.* **2011**, *9*, 5641−5644.
(21) Lee, J.-W.; Serna, F.; Nickels, J.; Schmidt, C. E. *Biomacromolecules* **2006**, *7*, 1692−1695.
(22) Miao, W. J.; Bard, A. J. *Anal. Chem.* **2003**, *75*, 5825−5834.
(23) Trmcic-Cvitas, J.; Hasan, E.; Ramstedt, M.; Li, X.; Cooper, M. A.; Abell, C.; Huck, W. T. S.; Gautrot, J. E. *Biomacromolecules* **2009**, *10*, 2885−2894.
(24) Bhattacharyya, D.; Gleason, K. K. *Chem. Mater.* **2011**, *23*, 2600−2605.
(25) Nie, G.; Zhou, L.; Guo, Q.; Zhang, S. *Electrochem. Commun.* **2010**, *12*, 160−163.
(26) Zhang, G.; Lu, B.; Wen, Y.; Lu, L.; Xu, J. *Sens. Actuators, B* **2012**, *171−172*, 786−794.
(27) Maciejewska, J.; Pisarek, K.; Bartosiewicz, I.; Krysiński, P.; Jackowska, K.; Bieguński, A. T. *Electrochim. Acta* **2011**, *56*, 3700−3706.
(28) Nie, G.; Zhang, Y.; Guo, Q.; Zhang, S. *Sens. Actuators, B* **2009**, *139*, 592−597.
(29) Nie, G.; Bai, Z.; Chen, J.; Yu, W. *ACS Macro Lett.* **2012**, *1*, 1304−1307.
(30) Kurusu, F.; Ohno, H.; Kaneko, M.; Nagasaki, Y.; Kataoka, K. *Polym. Adv. Technol.* **2003**, *14*, 27−34.
(31) Yaseen, M.; Ali, M.; Najeebullah, M.; Munawar, M. A.; Khokhar, I. *J. Heterocycl. Chem.* **2009**, *46*, 251−255.
(32) Guirado, G.; Coudret, C.; Hliwa, M.; Launay, J.-P. *J. Phys. Chem. B* **2005**, *109*, 17445−17459.
(33) Tao, L.; Mantovani, G.; Lecolley, F.; Haddleton, D. M. *J. Am. Chem. Soc.* **2004**, *126*, 13220−13221.
(34) Dong, H.; Li, C. M.; Chen, W.; Zhou, Q.; Zeng, Z. X.; Luong, J. H. T. *Anal. Chem.* **2006**, *78*, 7424−7431.
(35) Baba, A.; Taranekar, P.; Ponnapati, R. R.; Knoll, W.; Advincula, R. C. *ACS Appl. Mater. Interfaces* **2010**, *2*, 2347−2354.
(36) Uygun, A. *Talanta* **2009**, *79*, 194−198.
(37) Maiti, J.; Pokhrel, B.; Boruah, R.; Dolui, S. K. *Sens. Actuators, B* **2009**, *141*, 447−451.
(38) Wen, Y.; Xu, J.; Liu, M.; Li, D.; Lu, L.; Yue, R.; He, H. *J. Electroanal. Chem.* **2012**, *674*, 71−82.
(39) Xu, J.; Nie, G.; Zhang, S.; Han, X.; Hou, J.; Pu, S. *J. Polym. Sci., Part A: Polym. Chem.* **2005**, *43*, 1444−1453.
(40) Nie, G.; Yang, H.; Wang, S.; Li, X. *Crit. Rev. Solid State Mater. Sci.* **2011**, *36*, 209−228.
(41) Nie, G.; Cai, T.; Zhang, S.; Bao, Q.; Xu, J. *Electrochim. Acta* **2007**, *52*, 7097−7106.
(42) Cho, E. J.; Lee, J.-W.; Ellington, A. D. *Annu. Rev. Anal. Chem.* **2009**, *2*, 241−264.
(43) Ramanavicius, A.; Ryskevic, N.; Oztekin, Y.; Kausaite-Minkstimiene, A.; Jursenas, S.; Baniukevic, J.; Kirlyte, J.; Bubniene, U.; Ramanaviciene, A. *Anal. Bioanal. Chem.* **2010**, *398*, 3105−3113.
(44) Ramanavicius, A.; Kurilcik, N.; Jursenas, S.; Finkelsteinas, A.; Ramanaviciene, A. *Biosens. Bioelectron.* **2007**, *23*, 499−505.
(45) Sullivan, B. P.; Salmon, D. J.; Meyer, T. J. *Inorg. Chem.* **1978**, *17*, 3334−3341.
(46) Zhang, J.; Qi, H. L.; Li, Y.; Yang, J.; Gao, Q.; Zhang, C. X. *Anal. Chem.* **2008**, *80*, 2888−2894.
(47) Turkevich, J.; Stevenson, P. C.; Hillier, J. *Discuss. Faraday Soc.* **1951**, *11*, 55−75.
(48) Ambrosi, A.; Castañeda, M. T.; Killard, A. J.; Smyth, M. R.; Alegret, S.; Merkoçi, A. *Anal. Chem.* **2007**, *79*, 5232−5240.
(49) Hurst, S. J.; Lytton-Jean, A. K. R.; Mirkin, C. A. *Anal. Chem.* **2006**, *78*, 8313−8318.
(50) Liu, J. W.; Lu, Y. *Nat. Protoc.* **2006**, *1*, 246−252.
(51) Randriamahazaka, H.; Sini, G.; Tranvan, F. *J. Phys. Chem. C* **2007**, *111*, 4553−4560.
(52) Lu, B.; Xu, J.; Fan, C.; Jiang, F.; Miao, H. *Electrochim. Acta* **2008**, *54*, 334−340.
(53) Lu, B.; Yan, J.; Xu, J.; Zhou, S.; Hu, X. *Macromolecules* **2010**, *43*, 4599−4608.
(54) Qin, L.; Xu, J.; Lu, B.; Lu, Y.; Duan, X.; Nie, G. *J. Mater. Chem.* **2012**, *22*, 18345−18353.
(55) Mazur, M.; Krysinski, P. *J. Phys. Chem. B* **2002**, *106*, 10349−10354.
(56) Nie, G.; Zhou, L.; Yang, H. *J. Mater. Chem.* **2011**, *21*, 13873−13880.
(57) Ruan, C. M.; Yang, L. J.; Li, Y. B. *Anal. Chem.* **2002**, *74*, 4814−4820.
(58) Hashimoto, K.; Ito, K.; Ishimori, Y. *Anal. Chem.* **1994**, *66*, 3830−3833.
(59) Wang, H.; Zhang, C. X.; Li, Y.; Qi, H. L. *Anal. Chim. Acta* **2006**, *575*, 205−211.
(60) Zhang, J.-J.; Zheng, T.-T.; Cheng, F.-F.; Zhang, J.-R.; Zhu, J.-J. *Anal. Chem.* **2011**, *83*, 7902−7909.
(61) Shen, L. H.; Li, X. X.; Qi, H. L.; Zhang, C. X. *Luminescence* **2008**, *23*, 370−375.
(62) Benoist, D. M.; Pan, S. *J. Phys. Chem. C* **2010**, *114*, 1815−1821.
(63) Zhou, B.; Xiao, X. L.; Xu, L. L.; Zhu, L.; Tan, L.; Tang, H.; Zhang, Y. Y.; Xie, Q. J.; Yao, S. Z. *Biosens. Bioelectron.* **2012**, *38*, 389−395.
(64) Zhang, J.-J.; Cheng, F.-F.; Zheng, T.-T.; Zhu, J.-J. *Anal. Chem.* **2010**, *82*, 3547−3555.
(65) Sheng, Z.; Hu, D.; Zhang, P.; Gong, P.; Gao, D.; Liu, S.; Cai, L. *Chem. Commun.* **2012**, *48*, 4202−4204.
(66) Bamrungsap, S.; Chen, T.; IbrahimShukoor, M.; Chen, Z.; Sefah, K.; Chen, Y.; Tan, W. *ACS Nano* **2012**, *6*, 3974−3981.